Acta Geologica Sinica (English Edition), 2021, 95(6): 1844–1856

Multi-objective Optimization of Geothermal Extraction from the Enhanced Geothermal System in Qiabuqia Geothermal Field, Gonghe Basin

SONG Guofeng[1], SONG Xianzhi[1,*], LI Gensheng[1], XU Ruina[2], CAO Wenjiong[3] and Zhao Chenru[4]

[1] *State Key Laboratory of Petroleum Resources and Prospecting, China University of Petroleum, Beijing 102249, China*
[2] *Key Laboratory for Thermal Science and Power Engineering, Ministry of Education, Key Laboratory for CO2 Utilization and Reduction Technology of Beijing, Department of Energy and Power Engineering, Tsinghua University, Beijing 100084, China*
[3] *Laboratory of Advanced Energy Systems, Guangdong Key Laboratory of New and Renewable Energy Research and Development, CAS Key Laboratory of Renewable Energy, Guangzhou Institute of Energy Conversion, Chinese Academy of Sciences (CAS), Guangzhou 510640, Guangdong, PR China*
[4] *Institute of Nuclear and New Energy Technology, Advanced Nuclear Energy Technology Cooperation Innovation Centre, Key Laboratory of Advanced Nuclear Engineering and Safety, Ministry of Education, Tsinghua University, Beijing 100084, China*

Abstract: A geothermal demonstration exploitation area will be established in the Enhanced Geothermal System of the Qiabuqia field, Gonghe Basin, Qinghai–Xizang Plateau in China. Selection of operational parameters for geothermal field extraction is thus of great significance to realize the best production performance. A novel integrated method of finite element and multi-objective optimization has been employed to obtain the optimal scheme for thermal extraction from the Gonghe Basin. A thermal-hydraulic-mechanical coupling model (THM) is established to analyze the thermal performance. From this it has been found that there exists a contraction among different heat extraction indexes. Parametric study indicates that injection mass rate (Q_{in}) is the most sensitive parameter to the heat extraction, followed by well spacing (*WS*) and injection temperature (T_{in}). The least sensitive parameter is production pressure (p_{out}). The optimal combination of operational parameters acquired is such that (T_{in}, p_{out}, Q_{in}, *WS*) equals (72.72°C, 30.56 MPa, 18.32 kg/s, 327.82 m). Results indicate that the maximum electrical power is 1.41 MW for the optimal case over 20 years. The thermal break has been relieved and the pressure difference reduced by 8 MPa compared with the base case. The optimal case would extract 50% more energy than that of a previous case and the outcome will provide a remarkable reference for the construction of Gonghe project.

Key words: geothermal energy, EGS, thermal performance, operational parameters, multi-objective optimization, Gonghe project

Citation: Song et al., 2021. Multi-objective Optimization of Geothermal Extraction from the Enhanced Geothermal System in Qiabuqia Geothermal Field, Gonghe Basin. Acta Geologica Sinica (English Edition), 95(6): 1844–1856. DOI: 10.1111/1755-6724.14875

1 Introduction

Geothermal energy is a renewable and environmentally friendly alternative to fossil fuel energy (Panwar et al., 2011; Sims, 2014). It is of great potential in residential heating and power generation (Lund et al., 2011). It is also especially abundant at depths of 3–10 km. However, deep geothermal resources have not been extensively developed due to challenges in technology and economics. An enhanced geothermal system (EGS) has been proposed to extract the heat from the deep earth (Samin, et al., 2019). Previous field experiments and geothermal demonstration projects have proved the concept of EGS but, even so, most EGS projects are abandoned due to inefficient production, huge human input, and uncertain risks (Giardini, 2009). Rosemanowes geothermal project in the UK was abandoned due to a thermal breakthrough (Samin, et al., 2019). Only one EGS project, the Soultz geothermal field in France, is barely being commercially operated among more than 40 EGS projects so far (Gérard et al., 2006). Therefore, it is necessary to carry out optimization research for geothermal exploitation to maximize the geothermal production and relieve phenomena such as thermal breakthrough.

Analysis of heat extraction performance is the premise for optimization of geothermal injection and production. The numerical method has proved a reliable and efficient tool to investigate geothermal performance (McDermott et al., 2006). Wang et al. (2020) studied the thermal performance of a novel open-loop geothermal system (OLGS) based on a thermal-hydraulic (TH) coupling model. OLGS in a horizontal well shows broader application prospects than in a vertical well. Qu et al. (2017) studied the influence of different fracture morphology on heat mining performance of an EGS based

* Corresponding author. E-mail: songxz@cup.edu.cn

on COMSOL which is a commercial finite element software (Qu et al., 2017) and found that complex fractures are favorable for heating the mining. Zeng et al. (2013a) numerically investigated heat production potential through two horizontal wells based on geological data at the Desert Peak geothermal field. Shi et al. (2019a) established a thermal-hydraulic-mechanical (THM) coupling model to analyze the effects of complex fracture network geometries on heat extraction efficiency for a multilateral-well enhanced geothermal system. Cao et al. (2016) compared the performances of a CO_2-EGS and a water-EGS and indicated that the thermal power of the CO_2-EGS is higher than that of the water-EGS under the same injection pressure but the service life of the former is shorter. Therefore, researchers have provided abundant models and simulation approaches to study the thermal performance of the geothermal system.

Other researchers have studied the optimization of geothermal development to obtain better performance. Wu et al. (2016) considered heat extraction from a multiple fracture system with double wells. They found the optimal ranges for a number of fractures and equal fracture spacing under a typical geothermal system, with ranges of 6 to 13 and 30 m to 90 m, respectively. Their single optimization objective is based on maximum outlet temperature. Asai et al. (2019) found exponential flow is the optimal water injection scheme for maximizing heat recovery of a double-well system over 30 years. However, it is thought that single objective optimization of geothermal performance may not acquire a balanced and feasible combination of operational parameters.

The optimization design for geothermal extraction is a typical multi-objective optimization problem (MOP) (Song et al., 2021). Various kinds of objectives are included in the MOP for geothermal exploitation. Juliusson and Bjornsson (2021) presented a mathematical framework, which has economic parameters coupled with an energy balance model, to optimize the size of a geothermal power plant. The optimal development strategy is found to be dependent on economic parameters (power price, well cost, power plant cost, etc.) and major characteristics of the reservoir (average well power, initial resource capacity and recharge). Samin et al. (2019) proposed a hybrid optimization approach that integrated finite element and genetic algorithms to improve the long-term performance of EGS reservoirs. The optimal objectives include the thermal power, total cost, and thermal drawdown. The maximum reservoir depth, the distance between the injection and production wells, and fluid injection pressure are optimally selected for both design and post-design of an EGS. Zhang et al. (2021) executed a thermal-hydraulic (TH) simulation for the large-scale geothermal energy exploitation in the Gonghe Basin, China. The performance of an intensive well placement was superior to an extensive well placement with higher production temperature and lower interruption in groundwater levels. Schulte et al. (2020) got a multiple-objective optimal design for a double-well system considering geological uncertainties based on experimental design-based proxy models. Biagi et al. (2015) utilized TOUGH2 and a multi-objective genetic algorithm to optimize the $SCCO_2$ injection rate to obtain higher thermal power.

Our earlier research developed a novel and integrated approach of finite element (FE), multiple regression (MR), non-dominated sorting genetic algorithm (NSGA-II), and the technique for order preference by similarity to an ideal solution (TOPSIS) (Song et al., 2021). The method is applied to an ideal multilateral-well hydrothermal system to obtain the optimal injection-production scheme under the constraints of water loss, thermal drawdown, and ranges of operational parameters and reservoir properties. The optimal case demonstrates a great improvement in production performance that the thermal breakthrough has been delayed by 1.1 years and the water loss decreased by 36.23%. However, rare research (Samin et al., 2019; Song et al., 2021) has explored the multi-objective optimization of the thermal performance considering underground multi-physics coupling processes in a real geological environment and geothermal project. It is also necessary to introduce a more complete coupling model considering the mechanical effect. Besides, there is no optimization study for geothermal extraction from the Qiabuqia field in the Gonghe Basin, a Cenozoic down-warped basin, which is located in the northeastern part of the Qinghai–Xizang (Tibetan) Plateau, where there are the most abundant geothermal resources in China. It is expected to establish a geothermal demonstration area in the Gonghe Basin in the future.

In this study, thermal extraction performance from the Gonghe demonstration area is optimized to obtain a suitable combination of operational parameters, such as injection temperature (T_{in}), mass injection rate (Q_{in}), production pressure (p_{out}), and well spacing (WS) under the constraints of surface pump pressure, system life, and ranges of operational parameters. The optimization objectives include electrical power, injection-production pressure difference, and recovery ratio. Firstly, we established and computed a THM coupling model to acquire the geothermal extraction performance of the triple-well EGS in the Qiabuqia geothermal field with the aim of investigating the effects of key operational parameters on geothermal extraction, including T_{in}, Q_{in}, p_{out} and WS. Then, we used multiple regression to gain objective functions with operational parameters. These functions were input to the NSGA-II algorithm. Finally, the aim was to acquire the optimal case to maximize the electrical power and recovery ratio and minimize the pressure difference. The thermal extraction performance of the base case, optimal case and the previous case are also compared. The optimal scheme would be expected to provide significant operational guidance for the efficient production of the Gonghe geothermal demonstration area.

2 Methodology

2.1 Method description

In our previous study (Song et al., 2021), a multi-objective optimization method was established to obtain the optimal and most suitable operation scheme for a hydrothermal system (Fig. 1). This research can also be extended to developments and optimization for EGS. In

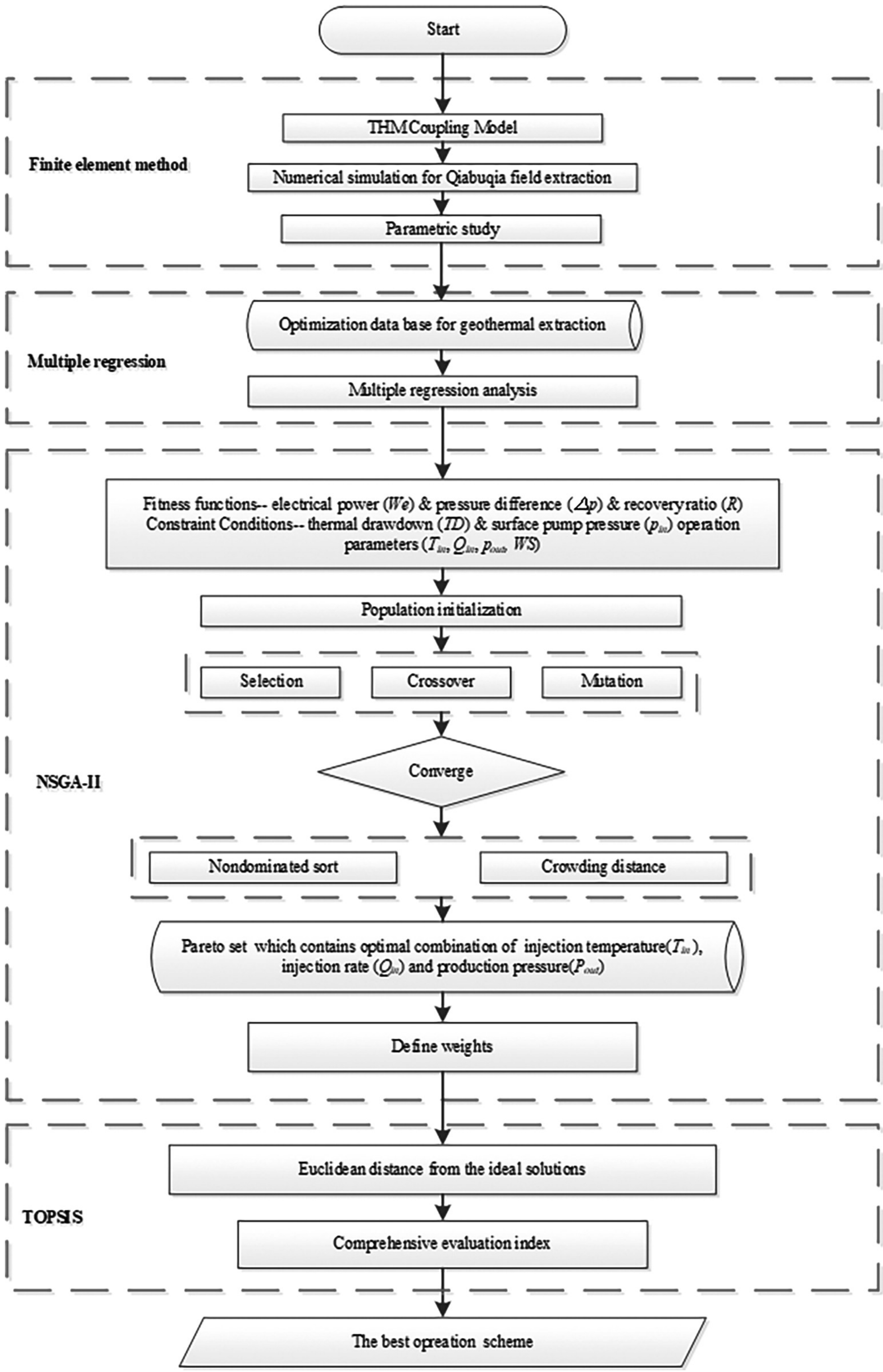

Fig. 1. Flowchart for the integration of FE, MR, NSGA-II and TOPSIS in the process of multi-objective optimization (from Song et al., 2021).

this approach, a THM coupling model is first established for field geothermal extraction. A parametric study is executed to get different production results under different operational parameters, such as T_{in}, Q_{in}, p_{out} and *WS*. Then, a multi-regression analysis is employed to establish functions of production characteristic results with injection -production parameters based on the parametric study. These functions are regarded as objective functions and constraint functions in the optimization algorithm. Then, the NSGA-II program (Deb et al., 2002) was adopted to get the Pareto solution (Chen et al., 2016), which contains an optimal combination of T_{in}, Q_{in}, p_{out} and WS under the constraints of thermal drawdown (TD), surface pump pressure (p_{in}) and the ranges of operation parameters. Finally, the TOPSIS method is used to make a comprehensive decision to select the most suitable scheme from the Pareto solution set for geothermal operators. A detailed introduction to NSGA-II and TOPSIS has been described previously (Yu et al., 2020; Song et al. 2021). Further details about optimization objectives and constraints will be described below.

2.2 Model assumptions

This study proposes an optimal injection and production scheme for geothermal extraction from the Gonghe demonstration plot. The first step is to describe geothermal production with a mechanical model. The following major assumptions are made:

(1) the matrix and fractures in reservoirs are represented based on discrete fracture networks (DFNs) (Kolditz and Clauser, 1998; Fox et al., 2015);

(2) the reservoir is homogeneous and isotropic (Shi et al., 2019b) and its formation physical properties remain constant;

(3) the heat and flow heat transfer in the wellbore are not included (Song et al. 2018). The chemical process is ignored;

(4) local thermal balance is employed for the heat transfer process in the matrix and fractures (Cao et al., 2016; Shi et al., 2019c);

(5) water stays in a liquid state under the operational conditions of the EGS (pressure is 20–50 MPa and temperature is 20–300°C). The variations of water property with temperate and pressure are referenced by COMSOL.

2.3 Governing equations

Heat extraction from the EGS is a complicated coupling process including fluid flow, heat transfer and rock deformation. In our previous research, a thermal-hydraulic -mechanical coupling model is developed. Detailed description can refer to the Appendix. The fluid flow in the rock matrix and fractures can be described by Darcy's law and mass conservation equations (Shi et al., 2019b). Artificial and natural fractures are considered as the main flow and heat transfer channels (Vik et al., 2018).The fracture permeability k_f (m^2) is expressed by a modified cubic law by introducing the transformation between the hydraulic opening and mechanical opening (Witherspoon et al., 1979):

$$k_f = \frac{{d_h}^2}{12} = \frac{\left(d_{h0} + \beta\left(d_f - d_{f0}\right)\right)^2}{12} \tag{1}$$

where d_h (m) is the hydraulic aperture that is used to compute the fracture conductivity; d_{h0} (m) and d_{f0} (m) represent the initial hydraulic aperture and initial mechanical aperture respectively; β denotes the irregularity of the fracture surface with a range generally from 0.5 to 1 (Witherspoon et al., 1979). Heat transfer in the matrix and fractures can be expressed with energy conversion equations (Song et al. 2018). Rock deformation is controlled by the elastic equations (from Shi et al., 2019a). Especially, u_n (m), as the normal displacement of fractures, is obtained by deformation equations and finally input to the fluid flow equation:

$$d_f = d_{f0} + u_n \tag{2}$$

A diagram to describe how the THM process is coupled is shown in Fig. 2. The p (Pa) induces the variation of effective stress. The temperature difference causes thermal stress. They both change the stress distribution and result in the matrix and fracture deformation. Permeability is enhanced due to the above deformation. The fluid flow and convective heat transfer are correspondingly affected. Finally, the heat extraction performance is remarkably affected. The THM model is well verified against the analytical solution in our previous studies (Shi et al., 2019b) and, therefore, the model reliablely describes the heat extraction from the Gonghe demonstration area.

3 Computation Model

3.1 Geological setting

The Gonghe Basin in the Qinghai–Xijang plateau of northwestern China contains abundant hot dry rock (HDR) geothermal resources (Liu et al., 2020). The Qiabuqia geothermal field is located in the eastern Gonghe Basin. It is estimated that the Qiabuqia geothermal field accounts for one-third of the total geothermal resources of the Gonghe Basin, which is probably > 200 billion tons of standard coal (Lei et al., 2019). A demonstration area for HDR extraction is promising in the Qiabuqia field. Current geothermal well distribution in the Gonghe Basin includes well GR1 drilled to 3705 m with a bottom temperature even reaching > 200°C. Our study carries out a geothermal performance analysis and optimization research for GR1 well because of its outstanding resources. Detailed geological information and temperature logs can be found in previous research (Lei et al., 2019; Lei et al., 2020).

3.2 Geometric model

Here we assume a triple-well fractured EGS for the Qiabuqia field based on previous data and research (Lei et al., 2019; Lei et al., 2020). Artificial hydraulic fracturing is employed to create a stimulated reservoir volume (SRV). Fig. 3 shows the system organization including HDR, SRV, fractures, and wells and detailed geometric parameters are listed in Table 1. The artificial fracture

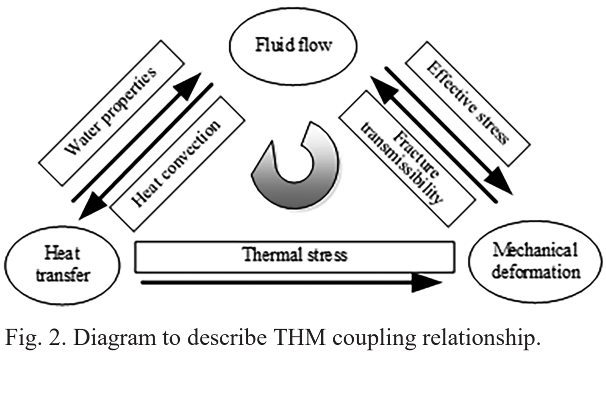

Fig. 2. Diagram to describe THM coupling relationship.

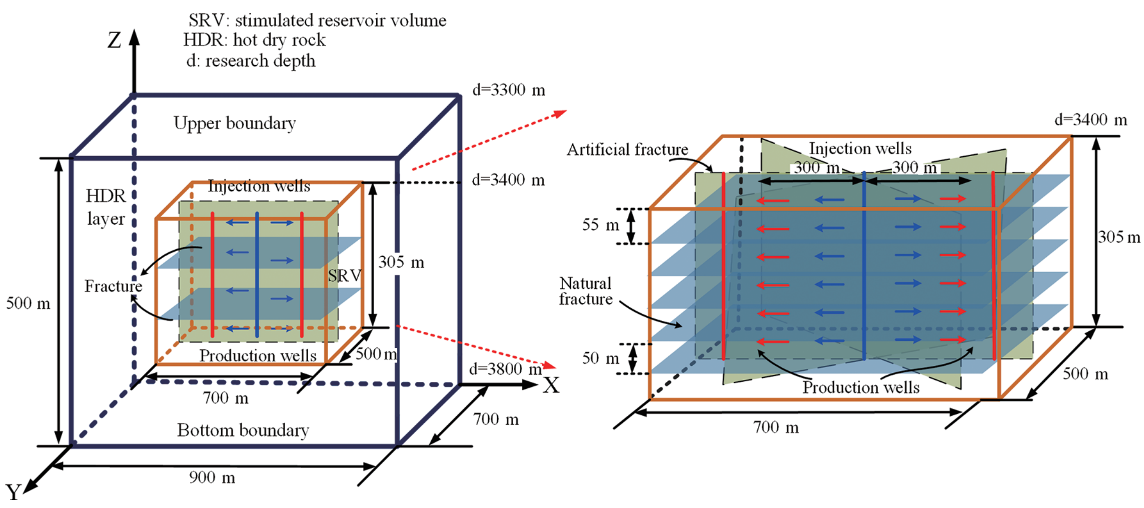

Fig. 3. Schematic diagram of the triple-well fractured EGS.
(a) system composition and distribution; (b) detailed distribution of wells and fractures in SRV.

length and height are 700 m and 305 m separately, as shown in Fig. 3a. Besides, five natural fractures are introduced to the SRV with dimensions of 700 m×500 m. The initial fracture mechanical width is assumed to be 0.5 mm. Moreover, the distribution of natural fractures is detailed in Fig. 3b.

3.3 Initial and boundary conditions

The geological data of the Gonghe reservoirs was obtained from previous drilling data and laboratory experiments on the Qiabuqia HDR granites. The formation and fracture properties are shown separately (Tables 2 and 3) and the initial and boundary conditions for the base case are given in Table 4. For the initial temperature distribution, the top temperature is 177.5°C at the depth of 3300 m and the temperature gradient is 0.07°C/m. The temperature at the bottom of well is about 200°C. There is no heat flux at the side boundary. The top and bottom of the HDR are both set as constant temperature boundaries, which equals the initial temperature. As for the distribution of pressure, it is 33 MPa at a depth of 3300 m with a pressure gradient of 8000 Pa/m. There is no fluid flow at the outer boundary of the HDR. the displacement field is a rigid boundary along the normal direction of the computation model because of the emphasis on the influence of temperature and pore pressure on the stress. As for the injection and production wells, stable mass Q_{in} and fixed p_{out} are adopted (Shi et al., 2019b). The constant mass Q_{in} and T_{in} are 30 kg/s and 60°C for the injection well, respectively. The stable p_{out} is 33 MPa. The simulation time of the THM coupling model is 20 years for heat extraction from the Gonghe demonstration area.

3.4 Solution mesh

The fully coupled THM model is computed and simulated in COMSOL, with a meshing scheme for a

Table 1 Model geometric parameters

Items	Values
HDR dimensions	900 m × 700 m × 500 m
SRV dimensions	700 m × 500 m × 305 m
Wellbore diameter	0.1 m
Artificial fracture	700 m × 305 m × 0.5 mm
Natural fracture	700 m × 500 m × 0.5 mm
Length of open hole section	305 m
Injection-production well spacing	300 m

Table 2 Physical properties of geothermal formation

Items	HDR	SRV
Porosity, φ_m	0.01	0.0354
Permeability, k_m	10^{-3} mD	0.5 mD
Density, ρ_s	2800 kg/m^3	2607 kg/m^3
Heat capacity, $C_{p,s}$	1000 J/(kg·K)	754.4 J/(kg·K)
Thermal conductivity, λ_s	3 W/(m·K)	2.51 W/(m·K)
Thermal expansion coefficient, α_T	5×10^{-6} K^{-1}	5×10^{-6} K^{-1}
Biot–Willis coefficient, α_B	0.7	0.7
Young's modulus, E	44.1 GPa	44.1 GPa
Poisson' ratio, v	0.23	0.23

Table 3 Physical properties of fracture (after Shi et al., 2019a, 2019b)

Items	Values
Porosity, φ_f	1
Mechanical Aperture, d_{f0}	0.5 mm
Hydraulic aperture, d_{h0}	2.45×10^{-5} m
Initial permeability, k_f	50 D
Density, ρ_s	2000 kg/m^3
Heat capacity, $C_{p,s}$	750 J/(kg·K)
Thermal conductivity, λ_s	2.5 W/(m·K)
Thermal expansion coefficient, α_T	5×10^{-6} K^{-1}
Biot–Willis coefficient, α_B	0.7
Young's modulus, E	44.1 GPa
Poisson' ratio, v	0.23
Coefficient of fracture irregularity, β	0.5

Table 4 Parameters of the initial and boundary conditions for the base case

Items	Values
Pressure at 3300 m subsurface	33 MPa
Pressure gradient	8000 Pa/m
Injection rate	30 kg/s
Production pressure (p_{out})	33 MPa
Temperature at 3300 m subsurface	177.5 °C
Temperature gradient	0.07 °C/m
Well spacing	300 m
Injection temperature	60°C

triple-well geothermal system for the Gonghe demonstration extraction (Fig. 4). An infinite domain with a width of 50 m is introduced to the four sides of the formation to represent a nearly extended geothermal reservoir, based on the spatial tension theory in COMSOL to produce refined free tetrahedral elements in the surrounding rock. As for the SRV, extremely refined triangular elements are generated on the bottom surface and swept to the top boundary along the z-axis. A total of more than 70,000 meshes were produced. A total heat production period of 20 years was studied.

3.5 Heat extraction evaluation index

Four evaluation indexes are introduced to quantitatively describe the production performance. Average production well temperature T_{out} is defined as the mean temperature of the production well interval. Thermal drawdown TD (K) equates to the difference between production temperature and initial temperature:

$$TD = T_{out}(t) - T_{out}(t_0) \tag{3}$$

where t_0 is the initial moment. We propose that production TD is no more than 10% during exploitation, which is also a measure of system lifetime (Zeng et al., 2013b). The average pressure difference Δp (MPa) equals the difference between average injection well pressure and production well pressure:

$$\Delta p = p_{in} - p_{out} \tag{4}$$

The larger the Δp, the more the pump consumption at the surface. Enthalpy change ΔH (J/kg) is defined as the difference between the produced enthalpy and injected enthalpy; NB. enthalpy is the sum of internal energy denoted by U and the product of volume and pressure, denoted by PV, expressed as H = U + PV (Zeng et al., 2013b):

$$\Delta H = C_{p,f}(T_{out}) \cdot T_{out} - C_{p,f}(T_{in}) \cdot T_{in} \tag{5}$$

Here, the enthalpy describes the internal energy per 1 kg water. $C_{p,f}$ (J/(kg·K)) is the specific heat capacity that varies with temperature. The higher the enthalpy change, the greater the geothermal performance. All produced heat is assumed to be used for power generation. The energy utilization efficiency is regarded as 0.45, which means 45% of thermal energy is transferred to electrical power. Electrical power W_e (MW) can be expressed as follows (Zeng et al., 2013b):

$$W_e = 0.45 q \Delta H \cdot \left(1 - T_{in}/T_{out}\right) \cdot 10^{-6} \tag{6}$$

where q (kg/s) is the mass rate and T_{in} (K) is reinjection temperature. The geothermal recovery ratio R (100%) is defined as the ratio of produced energy to maximum recoverable energy for reservoirs,

$$R = \frac{\iiint_{V_s} \rho_s C_{p,s}\left(T_i - T(t)\right) dV}{\iiint_{V_s} \rho_s C_{p,s}\left(T_i - T_{in}\right) dV} \tag{7}$$

where V_s (m^3) is the volume of stimulated reservoirs. The larger R indicates more thermal energy is extracted and the geothermal system is exploited to a greater extent.

4 Results and Discussion

4.1 Thermal performance of the base case

The evolution of the average production temperature and pressure difference during 20 years for the base case is shown in Fig. 5. The maximum temperature is 195°C, which is stabilized for about 4 years and then gradually decreases to 155°C over 20 years. The thermal drawdown is 30°C, which exceeds 10% of the initial production temperature. On the other hand, the injection-production pressure difference shows a sharp increase followed by a slow increase. This is because the low-temperature injection would lead to a steep increase in water viscosity. The maximum pressure difference would reach 18.4 MPa, which might be a test of the surface pump.

Electrical power and the recovery ratio vary during 20 years for the base case (Fig. 6). The maximum electrical power is 2.7 MW in the second year of exploitation. After two years, its value is on the decline and the minimum power is about 1.4 MW in the 20th year. For the variation of the recovery ratio, it keeps a linear growth during the extraction period. Some 14.4% of geothermal energy would be exploited from the Gonghe demonstration plot and, therefore, the electrical power of the base case is promising. However, it might not be feasible because of

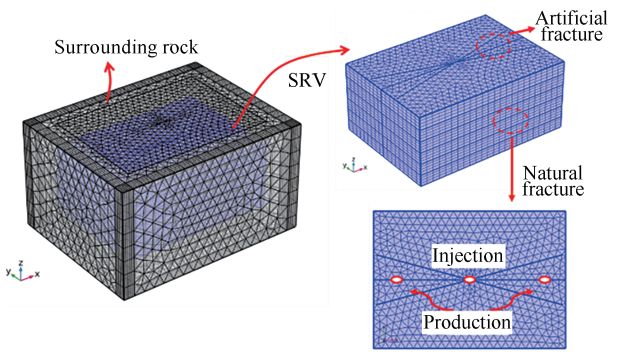

Fig. 4. Meshing scheme of a triple-well geothermal system for the Gonghe demonstration extraction.

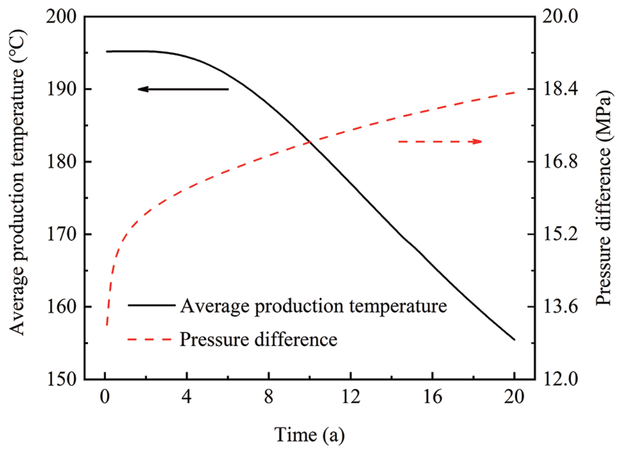

Fig. 5. Variations of average production temperature and pressure difference for the base case.

the larger pressure difference and thermal drawdown, which mean more human input and overdevelopment, respectively. Besides, according to the trend analysis, it is inferred that the four indexes mainly exhibit monotony during the 20 years. Therefore, based on the data from the same year, geothermal performance can be compared as the same as the 20th year.

4.2 Results of parametric study

The settings of the parametric cases are in bold numbers representing the base case in Table 5. In this section we mainly study the influence of operational parameters on the performance of heat extraction in the Gonghe demonstration area. Operation parameters include T_{in}, p_{out}, Q_{in}, and WS. Production variables such as electrical power, pressure difference and recovery ratio of the 20th year are input to make regression with the operation parameters. Here, the geothermal performance index of the 20th year is selected because of its monotonousness, as explained in the former section.

The variations of geothermal performance in the 20th year comprise Q_{in} (10–60 kg/s), T_{in} (40–90°C), p_{out} (30–35 MPa), and well spacing (150–350 m) (Figs. 7–10). For the electrical power, there occurs an optimal Q_{in} range of 20–30 kg/s (Fig. 7). This is because the electrical power is also dependent on the output temperature, as interpreted in equation (6). The higher Q_{in} will result in thermal breakout and temperature drop. In addition, the geothermal system with lower T_{in} and longer WS would result in higher electrical power. This is because the injection-production temperature difference is enhanced, which is the so-called enthalpy increase ΔH that is boosted. As for the pressure

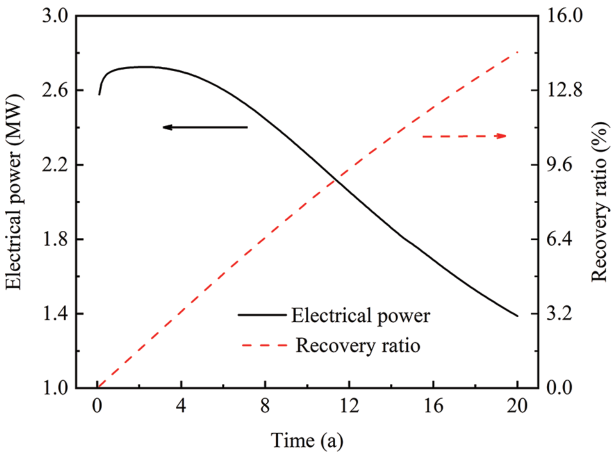

Fig. 6. Variations of electrical power and recovery ratio for the base case.

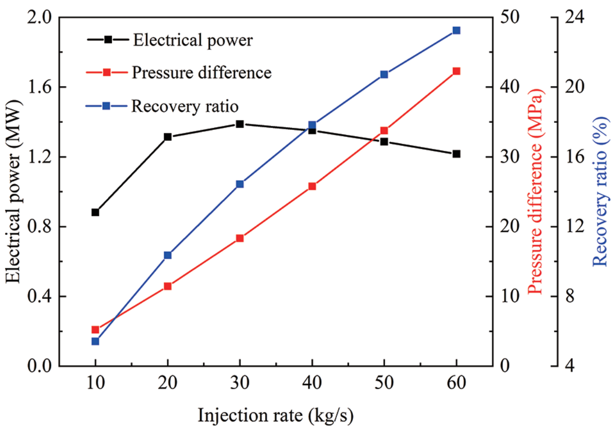

Fig. 7. The influence of Q_{in} on geothermal performance.

Table 5 Parametric experiments

Symbol	Operation parameters	Value
T_{in}	Injection temperature (°C)	40,50,60,70,80,90
p_{out}	Production pressure (MPa)	30,31,32,33,34,35
Q_{in}	Injection rate (kg/s)	10,20,30,40,50,60
WS	Well spacing (m)	150,200,250,300,350

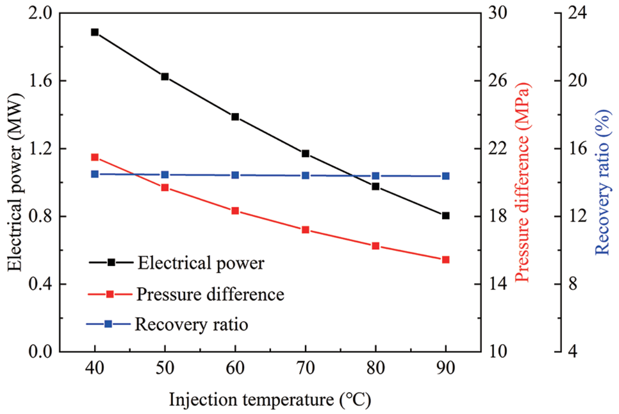

Fig. 8. The influence of T_{in} on geothermal performance.

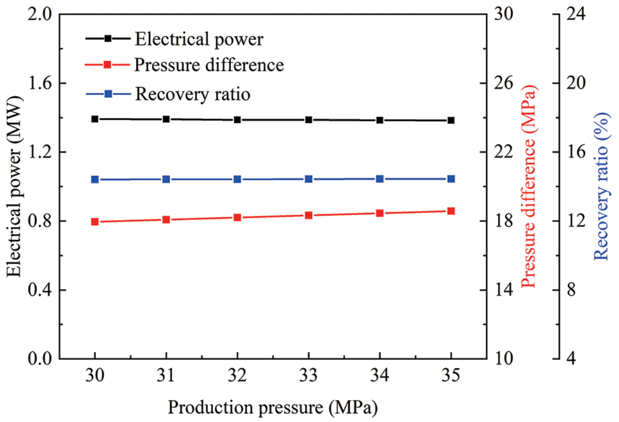

Fig. 9. The influence of p_{out} on geothermal performance.

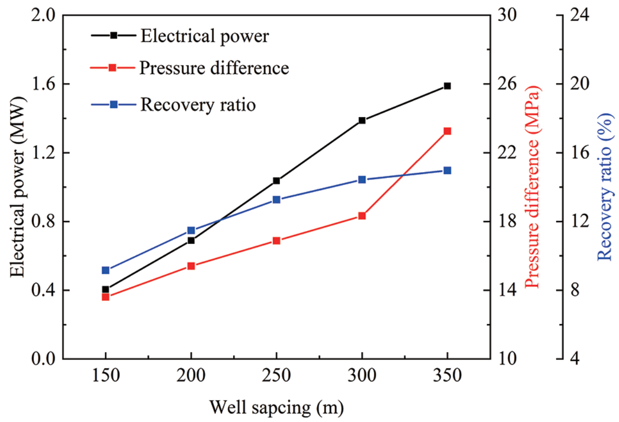

Fig. 10. The influence of WS on geothermal performance.

difference, the system with lower Q_{in}, higher T_{in}, and lower WS shows a lower human input (Figs. 7, 8 and 10). This can be explained by the reduction in the flow impedance during extraction. As for the recovery ratio, the geothermal system with larger Q_{in} and WS shows a higher exploitation degree. This is because the low-temperature controlling volume is enhanced. However, there is little influence of T_{in} on the recovery ratio. In fact, the recovery ratio is a relative value, as explained by equation (7). The larger T_{in} corresponds to a larger production temperature, which results in an approximately equal injection-production temperature difference. The variation lines are horizontal (Fig. 9), which indicates that there is little influence of p_{out} on geothermal extraction performance. This is because the variable values of p_{out} will change the absolute value of reservoir pressure but not the relative pressure difference under the stable Q_{in}. Therefore, the production dynamic performance will be hardly affected.

It is inferred that Q_{in} and WS would make a great contribution to the geothermal extraction variation. T_{in} contributes to a secondary degree of importance and p_{out} is the least important. In addition, small changes in operational parameters will lead to large changes in the system extraction performance. Nevertheless, it is incorrect to consider that a higher Q_{in} would lead to better extraction performance. There is a suitable range of Q_{in} (20–30 kg/s) to get a higher W_e, whereas the higher Q_{in} will enhance the recovery ratio and lower Q_{in} will reduce the pressure difference. The same phenomenon exists for the T_{in}, WS and p_{out}. Engineers should select different combinations of T_{in}, WS and p_{out} to optimize geothermal production under constraints such as reservoir properties and engineering parameters.

We also conclude that the evaluation indexes of geothermal performance can be divided into two categories based on the evolution of the characteristic heat extraction indexes, one a positive index and the other a negative index. The higher the positive index or the lower the negative index, the better the heat extraction performance. Here, the electrical power and recovery ratio both belong to the positive indexes whereas the pressure difference belongs to the negative index. As shown in Figs. 7–10, the two sorts of indicators are contradictory; however, this is an impossible phenomenon that the positive indexes are largest when the negative indexes are lowest. This contradiction among the different indexes of geothermal performance determines the need for multi-objective optimization rather than single-objective optimization. The necessity of multi-objective optimization is proven in the following sections.

The dimensional influence is necessary to reveal the sensitivity of geothermal extraction performance to the four different operational parameters (Figs. 7–10). Standard regression is employed to get the dimensionless influence of operational parameters. First, we establish a dimensional database according to the parametric study and curves. Then, each datum is standardized using the 0–1 standardized method (Song et al., 2021). Finally, multiple linear regression is taken to obtain dimensionless equations and coefficients (Table 6). Take electrical power W_e as an example; dimensionless electrical power W_{ed} can be expressed as follows:

$$W_{ed} = 0.26 - 0.68T_{ind} - 0.04p_{outd} + 0.09Q_{ind} + 0.83WS_d \quad (8)$$

The absolute value of the coefficient can be regarded as sensitivity. The sensitivity of WS and T_{in} on dimensionless W_e is 0.83 and 0.68, respectively. Fig. 11 shows the sensitivity of operational parameters to the geothermal extraction performance. In general, Q_{in} is the most sensitive parameter, followed by WS and T_{in} and the least sensitive parameter is p_{out}. The dimensionless order of sensitivity is consistent with the previous parameterized curves. Q_{in}, WS and T_{in} would be focused in further optimization research.

4.3 Results of multi-objective optimization

4.3.1 Objective functions

Parametric cases provide simulation results that form an optimization database to establish optimization objective functions. Simulation results cannot be applied directly to the optimization algorithm NSGA-II. Here, dimensional functions of W_e, Δp and R with operational parameters are established as equations (9), (10) and (11).

$$W_e = a_0 + a_1T_{in} + a_2P_{out} + a_3Q_{in} + a_4WS + a_5WS^2 \quad (9)$$

$$\Delta p = b_0 + b_1T_{in} + b_2P_{out} + b_3Q_{in} + b_4WS \quad (10)$$

$$R = c_0 + c_1T_{in} + c_2P_{out} + c_3Q_{in} + c_4WS + c_5Q_{in}^{\ 2} + c_6WS^2 \quad (11)$$

Sample regression is adopted to determine the formation of equations (Song et al., 2021). The detailed coefficients of the optimization equations are listed in Table 7 and relevant statistical parameters of multiple regression can be found in Table 8. The closer the Multiple R and R Square are to 1, the higher the correlation. The lower the standard deviation, the larger the degree of the fit. The p value is the result of an F test

Table 6 Dimensionless sensitivity of operational parameters on thermal performance

Dimensionless operational parameters	Coefficients in equation Δp_d	Coefficients in equation W_{ed}	Coefficients in equation R
T_{ind}	−0.17	−0.68	0.01
p_{outd}	0.03	−0.04	−0.01
q_{ind}	1.00	0.09	0.97
WS_d	0.21	0.83	0.33

Table 7 Coefficients for objective functions

Coefficient a	Value	Coefficient b	Value	Coefficient c	Value
a_0	−0.1252	b_0	−15.0892	c_0	−15.9327
a_1	−0.0211	b_1	−0.1239	c_1	−0.0019
a_2	0.0449	b_2	0.2227	c_2	0.0048
a_3	0	b_3	0.7438	c_3	0.5705
a_4	0.0065	b_4	0.0394	c_4	0.0895
a_5	−0.0006	-	-	c_5	−0.0031
-	-	-	-	c_6	−0.0001

Table 8 Statistical parameters of multiple regression

Statistical parameters	We	Δp	R
Multiple R	0.98824	0.99505	0.99988
R Square	0.97662	0.99013	0.99977
Standard deviation	0.97039	0.98750	0.99966
P	4.85574E-12	7.63531E-15	7.74914E-23

that is a necessary step to check the regression effect. Here, p values are all much less than the significance level of 0.05. To sum up, three optimization objective functions are reliable to input to the NSGA-II.

4.3.2 Description and solution of a multi-objective optimization problem

A complete optimization problem includes optimization objectives, decision variables and constraints. This study focuses on the optimization of geothermal extraction performance for the Gonghe demonstration area to recommend an optimal scheme for field exploitation. Three objectives are selected to be optimized simultaneously: the aim is to maximize W_e, minimize Δp and maximize recovery ratio R; the decision variables are operational parameters such as T_{in}, P_{out}, Q_{in}, and WS. The major constraints include surface pump capacity, geothermal production life, range of operational parameters. The bottom injection pressure is proposed not to exceed 50 MPa at 3000 m underground considering the capacity of the surface pump. TD is advised not to exceed 10% of the initial production temperature (Zeng et al., 2013b). The mathematical description of the optimization problem can be expressed as equations (12).

$$[x]^T = [T_{in}\ Q_{in}\ p_{out}\ \mathrm{WS}]^T$$
$$\min f(x) = (-W_e(x), \Delta p(x), -R(x))$$
$$s.t \begin{cases} [x]^T = [T_{in}\ Q_{in}\ p_{out}\ \mathrm{WS}]^T \\ lb = [40\ 10\ 30\ 150], ub = [90\ 60\ 35\ 350] \\ 175 \le T_{out} \le 195, p_{in} < 50 \end{cases} \quad (12)$$

NSGA-II is used to solve multi-objective optimization problems, with the algorithm settings in Table 9. There is a total of 10000 iterations. Each iteration produces 1000 individuals after optimization operations like the selection, crossover, mutation, non-dominated sort, and computing crowding distance. Finally, the last generation with 1000 combinations of operational parameters makes up the Pareto solution set.

Each blue point in the optimal solution set for geothermal extraction from the Gonghe demonstration area (Fig. 12) represents a possible optimal scheme. The ranges of operational parameters can be identified according to the 1000 blue points (Table 10). The ranges can provide ideas for the initial design of the Gonghe injection and production. Note that the range of Q_{in} is narrowed down to 10–30.22 kg/s and the range of WS is narrowed down to 262.57–300 m.

Table 9 Parameters for NSGA-II

Parameters in NSGA-II	Value
Population size	1000
Number of iterations	10000
Function tolerance	1E-5
Number of decision variables	4
Selection function	Tournament size 2 and crowding distance
Crossover function	Single point
Crossover probability	0.35
Mutation probability	0.1

TOPSIS is employed to get an exact and unique scheme for the Gonghe injection and production. 1000 points are numbered. The comprehensive evaluation index for each scheme is calculated based on the TOPSIS method, as shown in Fig. 13. The red point equates to the largest value of 0.753. Corresponding operational parameters are that (T_{in}, p_{out}, Q_{in}, WS) equals (72.72°C, 30.56 MPa, 18.32 kg/s, 327.82 m), respectively.

4.4 Comparison of heat performance among different cases

4.4.1 Comparison between the optimal and base cases

The comparison of geothermal extraction performance between the base case and optimal case is shown in Figs. 14 and 15. Regarding the average production temperature (Fig. 14), the base case shows a steep thermal drawdown compared with the optimal case, with a lifetime of 12.5

Table 10 Optimal ranges of operational parameters for geothermal extraction from the Gonghe demonstration area

Operational parameters	Range
T_{in}	40–90°C
p_{out}	30–32.93 MPa
Q_{in}	10–30.22 kg/s
WS	262.57–350 m

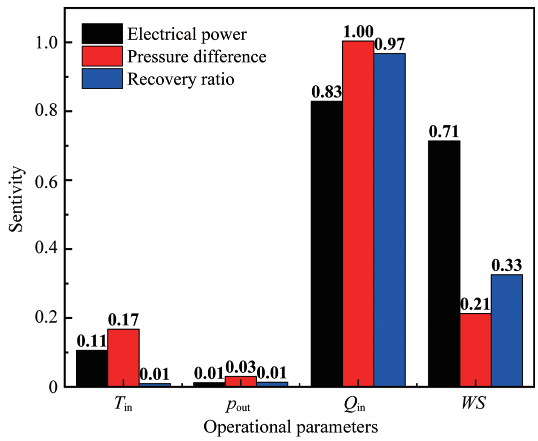

Fig. 11. Sensitivity of operational parameters on geothermal extraction performance.

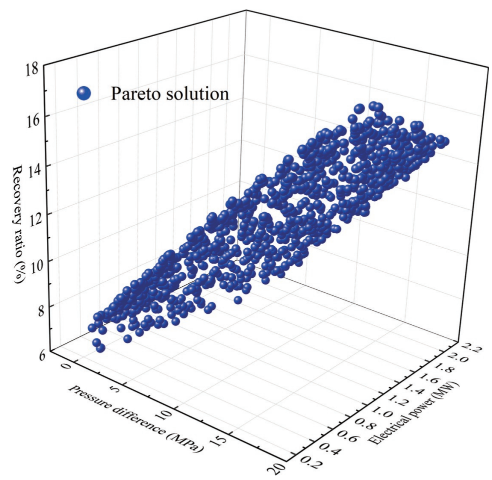

Fig. 12. Pareto solution set of operational parameters for geothermal extraction from the Gonghe demonstration.

years according to the 10% *TD* whereas the system can last more than 20 years in the optimal case. The average production temperature is 182.8°C and is enhanced by 27.3°C after 20-year extraction. W_e shows a much slower downward trend and its largest value is 1.41 MW, which decreases to 1.13 MW after a 20-year period; that is 0.25 MW (18%) lower than that of the base case. The pressure difference is 10.24 MPa, which is 8.01 MPa (44%) lower than that of the base case. Therefore, the optimal case significantly delays the thermal breakout and reduces the human input of injection pressure although the W_e decreases to a lower extent. The selection of the base case is uncertain because it is not feasible, as explained in section 2. The optimal case shows higher reliability and better performance through scientific optimization and decision.

4.4.2 Comparison between the optimal and previous cases

Lei et al. (2019) proposed an injection-production scheme for the Gonghe demonstration area based on TOUGH, another reliable commercial finite-element software for geothermal extraction. The same well pattern is adopted here. Comprehensive parametric studies were carried out to get suitable operational parameters. The T_{in}, p_{out}, Q_{in} and *WS* are 60°C, 30MPa, 10kg/s, 300 m, respectively, as Lei et al. (2019) proposed. The comparison of thermal extraction performance between the optimal case and the previous case is shown in Figs. 16 and 17. As for the average production temperature, the optimal case shows a larger thermal drawdown and the T_{out} is 9.4°C lower than that of the previous case. Nonetheless, both geothermal systems have a lifetime of more than 20 years. As for the pressure difference, the previous case shows a lower value, which is 5.1 MPa less than that of the optimal case. The bottom injection pressure would/will not exceed 50 MPa either for the optimal case. Therefore, both cases satisfy the constraint requirements and the previous case shows lower human input according to pressure difference. As for the W_e, its value in the optimal case is always larger than that of the previous case during the 20 years and it is 0.24 MW (27%) more in the 20th year. As for the recovery ratio, the optimal case extracts 9.7% of thermal energy from reservoirs with 50% more energy exploited than that of the previous example. Therefore, geothermal energy has been utilized to a greater extent under the same condition of surface pump constraints after multi-objective optimization.

4.4.3 Temperature distribution for different cases

There is a significant difference in low-temperature clouds among different cases after 20 years (Fig. 18). The order of low-temperature areas is the previous case, optimal case, and base case. A summary of thermal performance for different cases over a 20 year span is seen in Table 11. This indicated that more energy is recovered under the base case, followed by the optimal case. The least energy is extracted under the previous example. However, the base case shows the most remarkable phenomenon of thermal breakthrough and the previous case presents thermal breakthrough to the least extent.

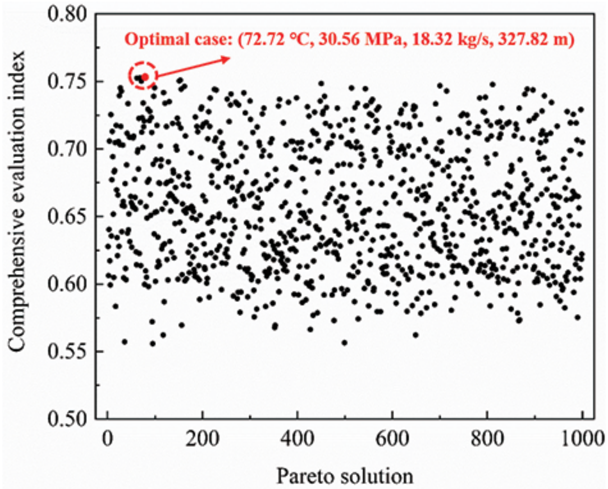

Fig. 13. Sorted optimal injection and production scheme based on TOPSIS (red = optimal case).

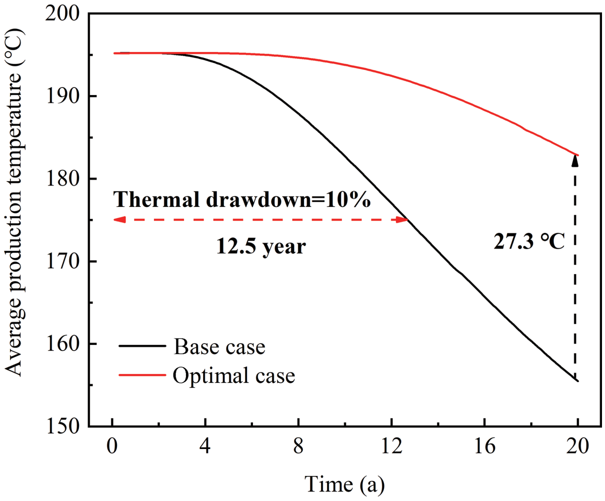

Fig. 14. Comparisons of T between the optimal case (red) and the base case (black).

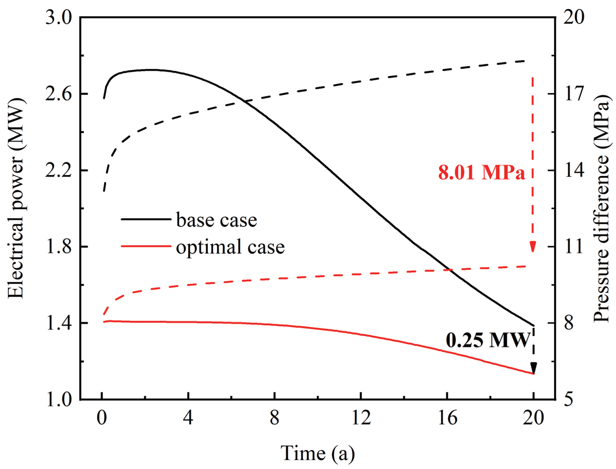

Fig. 15. Comparisons of W_e and $\triangle p$ between the optimal case (red) and base case (black).

Therefore, the base case is not feasible and the previous case does not make full use of the geothermal energy. The former is extreme and the latter is conservative. In short, the optimal case presents better thermal performance. The multi-objective optimization method is proved to be reliable, practical, and efficient enabling a balanced geothermal production to be realized.

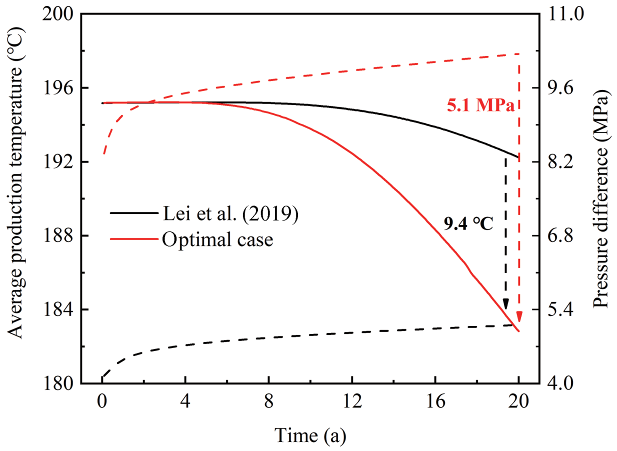

Fig. 16. Comparison of T_{out} and $\triangle p$ between the optimal case and the previous case.

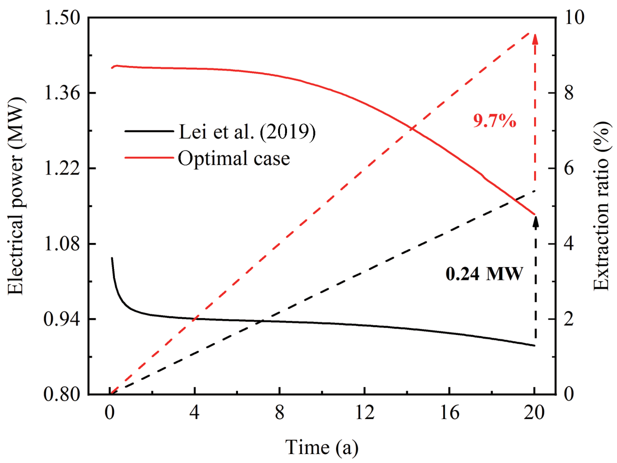

Fig. 17. Comparison of W_e and R between the optimal case and the previous case.

5 Conclusions

In this research, an integrated multi-objective optimization method was employed to obtain the optimal operation scheme for heat extraction from the Gonghe demonstration area. The effects of key operational parameters on Gonghe geothermal extraction were ascertained, including injection temperature (T_{in}), injection mass rate (Q_{in}), production pressure (p_{out}) and well spacing (WS). The optimal scheme was acquired taking into account multiple constraints of the surface pump, geothermal system life, and ranges of operation parameters. The thermal extraction performances of the base case, optimal case and the previous case were also compared. The proposed scheme would be expected to provide best-practice operational guidance to the production of the Qiabuqia geothermal field. Key conclusions are drawn as follows:

(1) there is a contraction among the evaluation indexes of thermal extraction performance. They are divided into two categories: one is the positive characteristic indexes like electrical power and recovery ratio; the other is negative index like pressure difference. The contraction among the thermal indexes determines the way of multi-objective optimization rather than single-objective optimization;

(2) parametric curves qualitatively indicate there exists an optimal range of Q_{in} (20–30 kg/s) to get higher electrical power. Dimensionless analysis quantitatively indicates that Q_{in} is the most sensitive parameter, followed by WS and T_{in}. The least sensitive parameter is p_{out}. The dimensionless influence degree for T_{in}, Q_{in}, p_{out}, and WS on electrical power are 0.68, 0.09, 0.04, and 0.83,

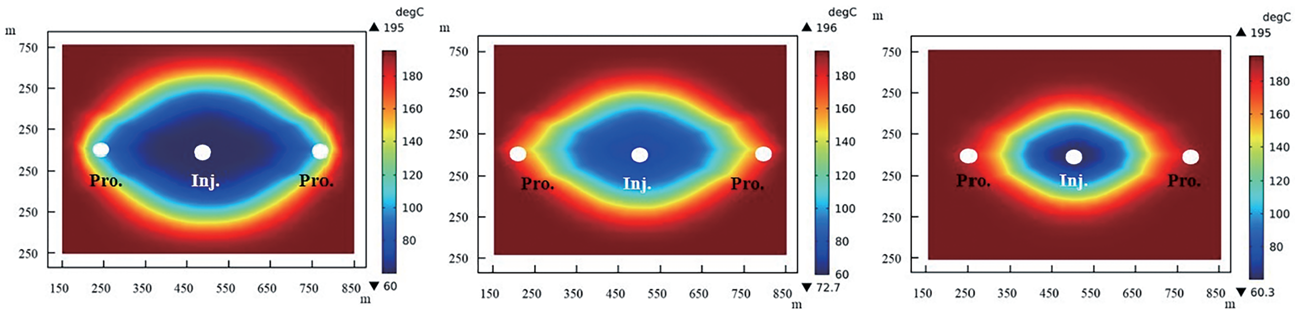

Fig. 18. Temperature cloud of selected horizontal fracture for the base case (left), optimal case (middle) and previous case (right) in the 20th year.

Table 11 Thermal performance comparision of different cases (t = 20 a)

Case type	Electrical power (MW)	Pressure difference (MPa)	System life (a)	Extraction ratio (%)	Comprehensive evaluation index	Qualitative evaluation
Base case	1.4	18	12.5	14.4	0.40	Extreme
Optimal case	1.15	10	> 20	10.4	0.42	Balanced
Previous case	0.89	5	> 20	7	0.39	Conservative

respectively. Q_{in}, WS and T_{in} are especially crucial in the optimization research;

(3) the Pareto solution provides the ranges of operational parameters for the Gonghe demonstration area. The range of Q_{in} is 10–30.22 kg/s and that of WS is 262.57 to 300 m. The optimization and decision result propose the optimal combination of operational parameters is (T_{in}, p_{out}, Q_{in}, WS), which equals (72.72°C, 30.56 MPa, 18.32 kg/s, 327.82 m);

(4) the optimal case shows higher feasibility and better thermal performance. This significantly delays the thermal breakout and reduces the human input of injection pressure compared with the base case. The lifetime of the Gonghe demonstration extraction is greater than 20 years according to the optimal case. The maximum W_e is 1.41 MW and the minimum W_e is 1.13 MW during a 20-year exploitation. The average production temperature is 182.8°C in the 20th year, which is enhanced by 27.3°C compared with the base case. The pressure difference is 10.24 MPa, which is 8.01 MPa lower than that of the base case. Comparison with the previous case shows that the latter produces higher electrical power, which is 0.24 MW more than that of the optimal case. However, the optimal case would extract 50% more energy from the reservoirs with a recovery ratio of 9.7%. Therefore, geothermal energy has been utilized to a greater extent under the same condition of surface pump constraints after multi-objective optimization.

In summary, the optimal case presents better thermal performance. The multi-objective optimization method is proved to be reliable, practical, and efficient to realize a balanced geothermal production.This study will provide a significant reference for geothermal sustainable exploitation in the Qiabuqia geothermal field. The optimization method is based on the multi-physics coupling model. Therefore, it is necessary to prove the production model considering more complicated geological information and a more complete heat extraction process in the future.

Acknowledgments

We would like to acknowledge the National Key R&D Program of China (Grant No. 2018YFB1501804), the National Natural Science Funds for Excellent Young Scholars of China (Grant No. 51822406), the Sichuan Science and Technology Program (2021YJ0389), the Program of Introducing Talents of Discipline to Chinese Universities (111 Plan) (Grant No. B17045), and the Beijing Outstanding Young Scientist Program (Grant No. BJJWZYJH01201911414038). Dr. Susan Turner (Brisbane) assisted with English language.

Manuscript received Jul. 28, 2021
accepted Sep. 27, 2021
associate EIC: XU Tianfu
edited by Susan TURNER and FEI Hongcai

Supplementary material to this article can be found online at http://doi.org/10.1111/1755-6724.14875.

Nomenclature

C_f	The fluid compressibility
$C_{p,f}$	The specific heat capacity of the fluid, J/(kg·K)
$C_{p,s}$	The rock specific heat capacity, J/(kg·K)
d_f	Fracture mechanical aperture, m
d_{f0}	The initial mechanical aperture, m
d_h	The hydraulic aperture, m
d_{h0}	The initial hydraulic aperture, m
E	Young's modulus, Pa
e	Volume strain
F_i	The body force per unit volume, N/m^3
G	Shear modulus, Pa
K_d	The drained bulk modulus of the porous matrix, MPa
k_f	The permeability of the fracture, m^2
k_m	The permeability of the rock matrix, m^2
L	The interval length, m
Q_1	The mass flux from rock matrix to fractures, kg/(m^2·s)
Q_2	The heat flux between the matrix and fracture, W/m^3
p	Pore pressure, Pa
p_{in}	The average injection well pressure, Pa
p_{out}	The average production well pressure, Pa
q	Mass rate, kg/s
R	Geothermal recovery ratio
S	The storage coefficient, Pa^{-1}
T	The temperature of rock and fluid, K
T_0	The initial temperature, K
T_{in}	Injection temperature, K
T_{out}	The mean temperature along production well interval, K
TD	Thermal drawdown, K
t	Time, s
t_0	The initial moment, s
$\boldsymbol{u}$	The flow velocity in the matrix, m/s
$\boldsymbol{u}_f$	The flow velocity in the fracture, m/s
u	Rock displacement, m
u_n	The normal displacement of fractures, m
V_s	The volume of stimulated reservoirs, m^3
W_e	Electrical power, MW

Greek symbols

μ_f	Fluid viscosity, Pa·s
ρ_f	Fluid density, kg/m^3
ρ_s	Solid rock density, kg/m^3
∇	The gradient operator along the tangential direction of the fracture
∇	The gradient operator along the normal direction of the fracture
α_B	The Biot–Willis coefficient
α_T	The thermal expansion coefficient, K^{-1}
φ	Porosity
δ_{ij}	The Kronecker symbol
β	The coefficient describing the transformation of two kinds of apertures
$(\rho C_p)_{eff}$	The effective volumetric heat capacity, J/(K·m^3)
λ_{eff}	Heat conductivity, W/(m·K)
λ_f	Fluid heat conductivity, W/(m·K)
λ_s	Solid heat conductivity, W/(m·K)
v	The Poisson's ratio
σ_e	The effective volumetric stress, Pa
σ_1	The first main stress, Pa
σ_2	The second main stress, Pa
σ_3	The third main stress, Pa
Δp	The pressure difference, Pa
ΔH	The difference between the produced enthalpy and injected enthalpy, J/kg

References

Asai, P., Panja, P., McLennan, J., and Deo, M., 2019. Effect of different flow schemes on heat recovery from Enhanced Geothermal Systems (EGS). Energy, 175: 667–676.

Biagi, J., Agarwal, R., and Zhang, Z., 2015. Simulation and optimization of enhanced geothermal systems using CO_2 as a working fluid. Energy, 86: 627–637.

Biot, M.A., 1962. Mechanics of deformation and acoustic propagation in porous media. Journal of Applied Physics, 33

(4): 1482–1498.
Cao, W.J., Huang, W.B., and Jiang, F.M., 2016. Numerical study on variable thermos physical properties of heat transfer fluid affecting EGS heat extraction. International Journal of Heat Mass Tran, 92: 1205–1217.
Cheng, W.L., Wang, C.L., Nian, Y.L., Han, B.B., and Liu, J., 2016. Analysis of influencing factors of heat extraction from enhanced geothermal systems considering water losses. Energy, 115: 274–288.
Deb, K., Pratap, A., Agarwal, S., and Meyarivan, T., 2002. A fast and elitist multiobjective genetic algorithm: NSGA-II. IEEE Transactions on Evolutionary Computation, 6(2): 182–197.
Fox, D.B., Koch, D.L., and Tester, J.W., 2015. The effect of spatial aperture variations on the thermal performance of discretely fractured geothermal reservoirs. Geothermal Energy, 3(1): 1–29.
Gérard, A., Genter, A., Kohl, T., Lutz, P., Rose, P., and Rummel, F., 2006. The deep EGS (Enhanced Geothermal System) project at Soultz-sous-Forets (Alsace, France). Geothermics, 35: 5–6.
Giardini, D., 2009. Geothermal quake risks must be faced. Nature, 462(7275): 848–849.
Juliusson, E., and Bjornsson, S., 2021. Optimizing production strategies for geothermal resources. Geothermics, 94(3): 102091.
Kolditz, O., and Clauser, C., 1998. Numerical simulation of flow and heat transfer in fractured crystalline rocks: Application to the hot dry rock site in Rosemanowes (UK). Geothermics, 27 (1): 1–23
Lei, Z.H., Zhang, Y.J., Yu, Z.W., Hu, Z.J., Li, L.Z., Zhang, S.Q., Fu, L., Zhou, N., and Xie, Y.Y., 2019. Exploratory research into the enhanced geothermal system power generation project: The Qiabuqia geothermal field, Northwest China. Renewable Energy, 139: 52–70.
Lei, Z.H., Zhang, Y.J., Zhang, S.Q., Fu, L., Hu, Z.J., Yu, Z.W., Li, L.Z., and Zhou, J., 2020. Electricity generation from a three-horizontal-well enhanced geothermal system in the Qiabuqia geothermal field, China: Slickwater fracturing treatments for different reservoir scenarios. Renewable Energy, 145: 65–83.
Liu, B., Zhao, H., Jin, H.L., and Chen, F.H., 2020. Holocene moisture variation recorded by aeolian sand-palaeosol sequences of the Gonghe Basin, Northeastern Qinghai-Tibetan Plateau, China. Acta Geologica Sinica (English Edition), 94 (3): 668–681
Lund, J.W., Freeston, D.H., and Boyd, T.L., 2011. Direct utilization of geothermal energy 2010 worldwide review. Geothermics, 40(3): 159–180.
McDermott, C.I., Randriamanjatosoa, A.R., Tenzer, H., and Kolditz, O., 2006. Simulation of heat extraction from crystalline rocks: The influence of coupled processes on differential reservoir cooling. Geothermics, 35(3): 321–344.
Panwar, N., Kaushik, S., and Kothari, S., 2011. Role of renewable energy sources in environmental protection: A review. Renewable and Sustainable Energy Reviews, 15(3): 1513–1524.
Qu, Z.Q., Zhang, W., and Guo, T.K., 2017. Influence of different fracture morphology on heat mining performance of enhanced geothermal systems based on COMSOL. International Journal of Hydrogen Energy, 42: 18263–18278.
Samin, M.Y., Faramarzi, A., Jefferson, I., and Harireche, O., 2019. A hybrid optimisation approach to improve long-term performance of enhanced geothermal system (EGS) reservoirs. Renewable Energy, 134: 379–389.
Schulte, D.O., Arnold, D., Geiger, S., Demyanov, V., and Sass, I., 2020. Multi-objective optimization under uncertainty of geothermal reservoirs using experimental design-based proxy models. Geothermics, 86: 101792.
Shi, Y., Song, X.Z., Li, J.C., Wang, G.S., Yulong, F.X., and Geng, L.D., 2019a. Analysis for effects of complex fracture network geometries on heat extraction efficiency of a multilateral-well enhanced geothermal system. Applied Thermal Engineering, 159: 113828.
Shi, Y., Song, X.Z., Li, G.S., Wang, G.S., Zheng, R., and Yulong, F.X., 2019b. Numerical investigation on heat extraction performance of a multilateral-well enhanced geothermal system with a discrete fracture network. Fuel, 244: 207–226.
Shi, Y., Song, X.Z., Wang, G.S., McLennan, J., Forbes, B., Li, X.J., and Li, J.C., 2019c. Study on wellbore fluid flow and heat transfer of a multilateral-well CO_2 enhanced geothermal system. Applied Energy, 249: 14–27.
Sims, R.E., 2014. Renewable energy and climate change mitigation: An overview of the IPCC Special Report. Weather Matters for Energy, 91–110.
Song, G.F., Song, X.Z., Li, G.S., Shi, Y., Wang, G.S., Ji, J.Y., Xu, F.Q., and Song, Z.H., 2021. An integrated multi-objective optimization method to improve the performance of multilateral-well geothermal system. Renewable Energy, 172: 1233–1249.
Song, X.Z., Shi, Y., Li, G.S., Yang, R.Y., Wang, G.S., Zheng, R., Li, J.C., and Lyu, Z.H., 2018. Numerical simulation of heat extraction performance in enhanced geothermal system with multilateral wells. Applied Energy, 218: 325–37.
Vik, H.S., Salimzadeh, S., and Nick, H.M., 2018. Heat recovery from multiple-fracture enhanced geothermal systems: The effect of thermoelastic fracture interactions. Renewable Energy, 121: 606–622.
Wang. G.S., Song, X.Z., Shi, Y., Zheng, R., Li, J.C., and Li, Z., 2020. Production performance of a novel open loop geothermal system in a horizontal well. Energy Conversion and Management, 206: 112478.
Witherspoon, P.A., Amick, C.H., Gale, J.E., and Iwai, K., 1979. Observations of a potential size effect in experimental determination of the hydraulic properties of fractures. Water Resources Research, 15(5): 1142–1146.
Wu, B.S., Zhang, X., Jeffrey, R.G., Bunger, A.P., and Jia, S.P., 2016. A simplified model for heat extraction by circulating fluid through a closed-loop multiple-fracture enhanced geothermal system. Applied Energy, 183: 1664–1681.
Yu, Z.T., Su, R.Z., and Feng, C.Y., 2020. Thermodynamic analysis and multi-objective optimization of a novel power generation system driven by geothermal energy. Energy, 199: 117381.
Zeng. Y.C., Su, Z., and Wu, N.Y., 2013a. Numerical simulation of heat production potential from hot dry rock by water circulating through two horizontal wells at Desert Peak geothermal field. Energy, 56: 92–107.
Zeng, Y.C., Wu, N.Y., Su, Z., Wang, X.X., and Hu, J., 2013b. Numerical simulation of heat production potential from hot dry rock by water circulating through a novel single vertical fracture at Desert Peak geothermal field. Energy, 63: 268–282.
Zhang, S.Y., Jiang, Z.J., Zhang, S.S., Zhang, Q.X., and Feng, G,H., 2021. Well placement optimization for large-scale geothermal energy exploitation considering nature hydro-thermal processes in the Gonghe Basin, China. Journal of Cleaner Production, 12: 128391.

About the first author

SONG Guofeng, male; born on February 1, 1996; Ph.D. candidate of the China University of Petroleum in Beijing; main research areas comprise multi-physics coupling mechanism in geothermal reservoirs and heat extraction optimization. E-mail: 15650797007@163.com

About the corresponding author

SONG Xianzhi, male; born on June 11, 1982; professor and doctoral supervisor of China University of Petroleum, Beijing; deputy director of State Key Laboratory of Petroleum Resources and Prospecting; acquired the NSFC National Outstanding Youth Fund in 2021; research interests include water jet, well drilling and completion, intelligent drilling, geothermal exploitation.